A Micromechanical Constitutive Model for the Dynamic Response of Brittle Materials "Dynamic Response of Marble"

Thesis by

Keith Haberman

In Partial Fulfillment of the Requirements
for the Degree of
Aeronautical Engineer

California Institute of Technology
Pasadena, California
2000
(Submitted June 1, 2000)

Acknowledgements

I always feel lucky to have had the opportunity to study and work at Caltech not only for the stimulating research environment but also for the people who made Caltech such a unique scientific community. Among others, my sincere gratitude goes to my advisor, Professor Ares J. Rosakis, for his guidance, support, and encouragement during the course of study. I am very grateful to Professor Rosakis for giving me the opportunity to pursue the work presented in this thesis. I would also like to thank Professor M. Ortiz for his support in this endeavor.

I am very grateful to my colleagues Joel Bennett and Steve Girrens at Los Alamos National Laboratory for their generous support in funding and resources. Without their support this endeavor would not have been possible.

Thanks are also due to all my fellow students and the staff in the Solids Mechanics Group of the Graduate Aeronautical Laboratories for their suggestions, comments, and assistance.

The work presented here was funded by Los Alamos National Laboratory and the Caltech Provost. This financial support is gratefully acknowledged.

Many sections in this thesis mirror the now famous report by Professor Ares J. Rosakis, "EXPLOSION AT THE PARTHENON: CAN WE PICK UP THE PIECES?" I am grateful to the individuals that contributed to this document, Dr. David M. Owen, Ms. Roussislava Zaharieva, Professor Ioannis Vardoulakis, and Professor George Exadaktylos.

Abstract

A micromechanically based constitutive model for the dynamic inelastic behavior of brittle materials, specifically "Dionysus-Pentelicon marble" with distributed microcracking is presented. Dionysus-Pentelicon marble was used in the construction of the Parthenon, in Athens, Greece. The constitutive model is a key component in the ability to simulate this historic explosion and the preceding bombardment form cannon fire that occurred at the Parthenon in 1678. Experiments were performed by Rosakis (1999) that characterized the static and dynamic response of this unique material. A micromechanical constitutive model that was previously successfully used to model the dynamic response of granular brittle materials is presented. The constitutive model was fitted to the experimental data for marble and reproduced the experimentally observed basic uniaxial dynamic behavior quite well. This micromechanical constitutive model was then implemented into the three dimensional nonlinear lagrangain finite element code Dyna3d(1998) Implementing this methodology into the three dimensional nonlinear dynamic finite element code allowed the model to be exercised on several preliminary impact experiments. During future simulations, the model is to be used in conjunction with other numerical techniques to simulate projectile impact and blast loading on the Dionysus-Pentelicon marble and on the structure of the Parthenon.

Table of Contents

1.0 Motivation / Introduction

On September 26, 1678, after heavy bombardment for several days a Venetian cannon ball penetrated the roof of the historic and famous Parthenon shown in Figure 1.0,

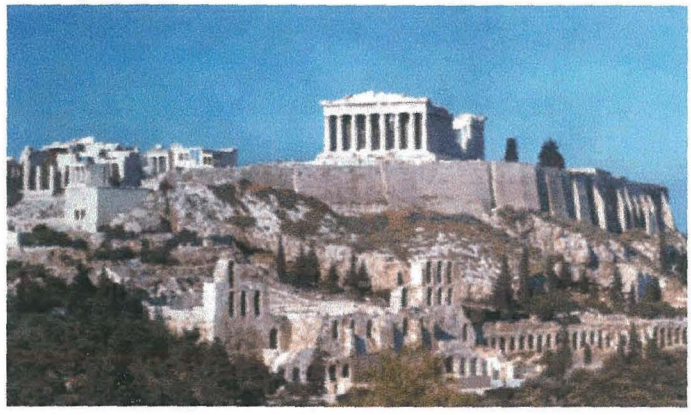

Figure 1.0 Parthenon

and ignited some of the black powder stored there by the Turks, causing an explosion and partially destroying part of the historic structure. Modern restoration efforts have focused on recreating this historic event using computer simulation in order to understand the extent of the damage inflicted on the structure. Specific issues of interest include quantification of localized damage to column drums by individual cannon balls, as well as thermal damage and cracking that has occurred through the centuries. With this goal in mind, an ambitious project was undertaken in the Graduate Aeronautical Laboratories at Caltech to determine the appropriate tools through multi-disciplinary historical, experimental, and computational research.

The ability to simulate cannon ball impact and recreate the explosion and resulting structural damage relies on the ability to experimentally characterize the complete dynamic response of the material, which in this case is, Dionysus-Pentelicon marble. Section 2.0 describes the mechanical properties of the Dionysus-Pentelicon marble in detail. Simulating the damage inflicted on the Parthenon requires an accurate physically based constitutive model capable of

predicting the complete response of the Dionysus-Pentelicon marble under both static and dynamic loading conditions. The micromechanically based constitutive model presented in Section 3.0 is such a model.

2.0 Mechanical Properties of Dionysus-Pentelicon Marble

This section describes the mechanical response of Dionysus-Pentelicon marble. The material is presented here for continuity and for experimental-simulation comparisons. The mechanical properties and the experimental methods are only briefly presented. Readers interested in the experiments and the techniques are referred to Rosakis (1999).

Dionysus-Pentelicon marble is a high quality white marble that was originally used in the construction of the Classical Parthenon. The marble can be described based on its three orthogonal geologic orientations, as shown in Fig. 2.1. The three directions are termed the "rift plane," along which strata can be observed; the "grain-plane", which defines the optimal plane for cutting the marble and finally, the "head-grain" plane. The strata, which are apparent in the photograph shown in Figure 2.1, are approximately 15 mm apart. In this report, the directions perpendicular to the rift, grain, and head grain planes will be termed the κ, M, and π directions, respectively. The marble is composed of approximately 98% calcite with less than 1% quartz. Its major physical and mechanical properties are given in Table 2.0.

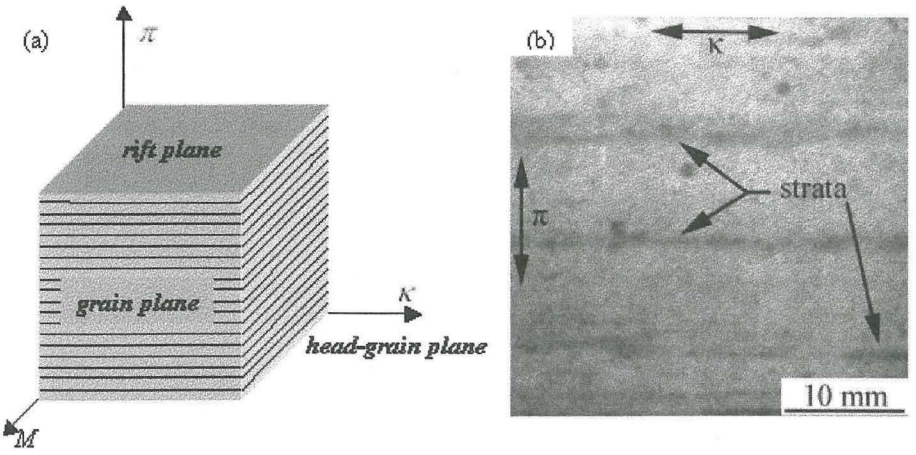

Figure 2.1 Schematic representations of the three planes and a photograph of the strata parallel to the rift plane.

Table 2.0 Selected physical and mechanical properties of Dionysus-Pentelicon marble.

Density, ρ (g cm^{-3})	2.75
Porosity, ϕ (%)	0.37
π Direction	
Young's Modulus, E_π (GPa)	81
Poisson's Ratio, ν_π	0.32
Longitudinal Wave Speed, c_l^π (m s^{-1})	6536
Shear Wave Speed, c_s^π (m s^{-1})	3369
Rayleigh Wave Speed, c_R^π (m s^{-1})	3131
κ and M Direction	
Young's Modulus, E_M (GPa)	78
Poisson's Ratio, ν_M	0.31
Longitudinal Wave Speed, c_l^M (m s^{-1})	6360
Shear Wave Speed, c_s^M (m s^{-1})	3310
Rayleigh Wave Speed, c_R^M (m s^{-1})	3071

The microstructure along each plane was investigated using optical microscopy. Figure 2.2 shows optical micrographs of specimens cut perpendicular to the three directions. In each orientation, large, equiaxed grains are observed. The average size of these grains were measured and found to be 400 μm in each orientation with the largest grains having dimensions of ~1 mm. It is also interesting to note that narrow twin-bands are observed within some of the grains in all orientations, most notably in the κ direction micrograph. Twinning refers to stress-induced diffusionless mass transport that occurs in some crystalline materials. These twins have, most probably, been formed during the process of geological formation and the associated large confining pressures. There was also evidence of some small pores and cracks in the microstructure.

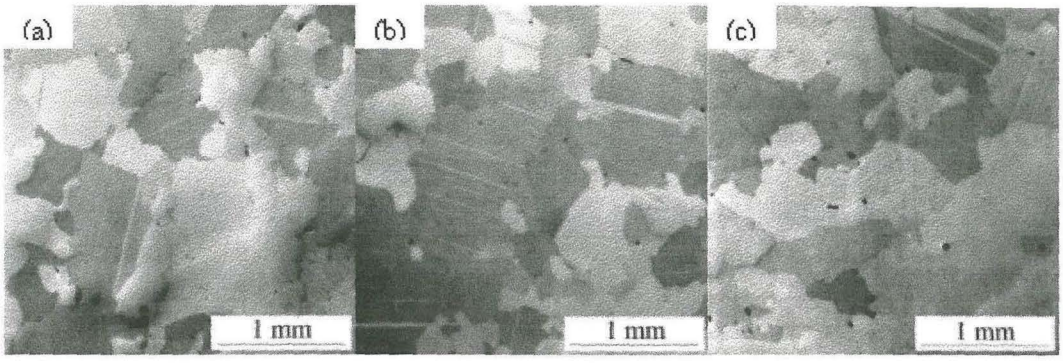

Figure 2.2 Optical micrographs of Dionysus-Pentelicon marble.

Numerical simulations of dynamic deformation and failure depend on reliable constitutive descriptions covering a wide range of strains and strain rates of the materials under consideration. Thus, as a first step, the stress-strain response of Dionysus-Pentelicon marble was determined as a function of strain rate using uniaxial compression tests. Generally, the constitutive (stress-strain) behavior of a material is widely recognized to be a function of strain, strain rate and temperature. The core of the constitutive response of a material is usually obtained from one-dimensional experiments conducted over a wide range of strain rates and temperatures and is then generalized to describe complete three-dimensional stress states.

The constitutive response of the Dionysus-Pentelicon marble was investigated by Rosakis (1999) in uniaxial compression at strain rates ranging over 10 orders of magnitude from 10^{-6} to 10^{4} s^{-1}. Figure 2.3 illustrates the effect of loading rate on the constitutive response with a plot of stress versus strain comparing three *M* orientation specimens.

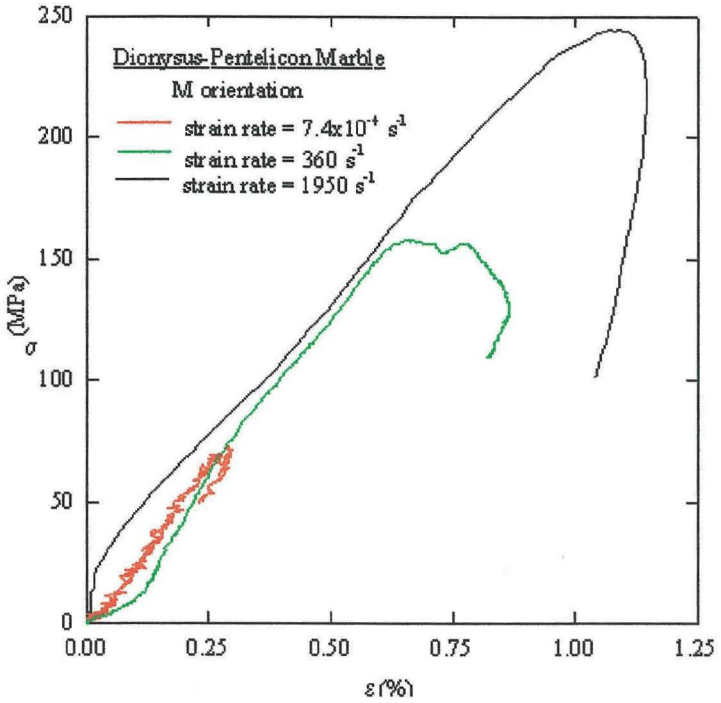

Figure 2.3 Stress versus strain for compressive loading parallel to the M orientation at strain rates by more than eight orders of magnitude.

The three experiments were conducted at three dramatically different strain rates of 7.4×10^{-4}, 300, and 1950 s^{-1}, spanning over eight orders of magnitude. From the figure, the effect of rate on the stress-strain behavior is clearly evident. At the lowest strain rate, the failure stress, taken as the peak stress, σ_p, is on the order of 50 to 100 MPa with strains to failure of less than 0.5%. Under dynamic loading conditions in the Hopkinson bar, the peak stress increases by a factor of up to five times, with a corresponding increase in the strain to failure. These features were observed consistently in experiments done in all three orientations.

The effect of orientation on constitutive response is illustrated in Figure 2.4, which shows stress-strain curves obtained at a strain rate of ~2000 s^{-1} for each of the three directions. The peak stress for all of the specimens lies in the range from 250 to 300 MPa. The κ and M orientations yield very similar results, whereas the higher peak stress corresponds to the π orientation specimen. The higher peak stress for the π orientation may result from the slightly higher strain rate, due to

the strain rate effect illustrated in Figure 2.3, or may be associated with a greater compressive strength in this orientation.

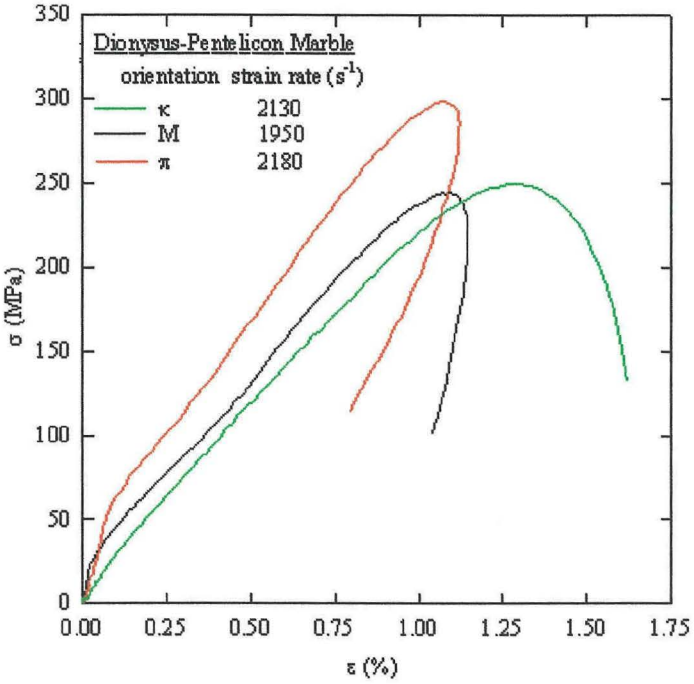

Figure 2.4 Stress-strain curves for the three orientations at an approximately constant strain rate of 2000 s^{-1}

Figure 2.5 provides a summary of all the compression experiments conducted thus far, plotted as peak compressive stress versus strain rate, including data obtained in each specimen orientation. The rate dependence of the failure stress is clearly evident in the figure: σ_p increases by a factor of seven, from 50 MPa at the lowest strain rate to 350 MPa. It appears that the data corresponding to the π orientation lies systematically above that obtained for the κ and M orientations. However the differences are on the order of the error and scatter in the measurements, indicating that any anisotropy is relatively weak.

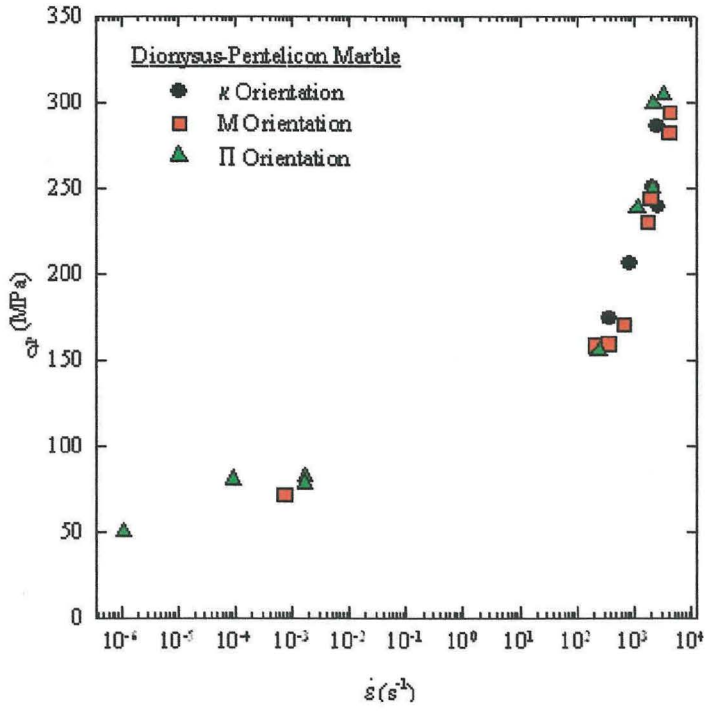

Figure 2.5 A plot of the variation of peak or failure stress with strain rate including data from all three orientations.

The apparent weakness of the anisotropy in the peak or failure stress is the primary motivation for an isotropic constitutive model presented in Section 3.0

3.0 Micromechanical Constitutive Model

In this section, the modeling of the dynamic constitutive response and damage evolution of the Dionysus-Pentelicon marble is described. A particular model is considered in which damage evolution is defined, quantified, and incorporated into the overall macroscopic constitutive behavior for a representative volume of material subjected to mechanical or thermal loading, $\dot{\varepsilon}_{ij}, \dot{\sigma}_{ij}, \dot{T}$. This mathematical model is formulated to represent the physics of the deformation and damage evolution processes. Due to the inherent dynamic nature of the problem, most equations are expressed in rate form. The model will be calibrated by using the experimentally obtained mechanical properties described in Section 2.0. It will then be implemented into an explicit nonlinear dynamic finite element code that will in turn be validated by comparison to idealized laboratory dynamic fracture problems. The validated codes will be used for modeling cannon ball impact events on column drums and, eventually, for the complete three dimensional simulation of the Morosini explosion. The model presented here is not intended to track the size and position of individual cracks in the material. It is formulated to give the average macroscopic damage response for a brittle material with a distribution of microcracks. The model given below is an adaptation of the brittle damage models of Addessio & Johnson (1990), Haberman *et al.* (1997) and Bennett *et al.* (1998).

Consider a brittle material that contains a distribution of natural flaws or cracks. In general, brittle materials experience damage accumulation under any type of mechanical loading, no matter how small or insignificant that loading may be. Figure 3.0 represents schematically the growth of an initial distribution of flaws or cracks under an arbitrary loading history.

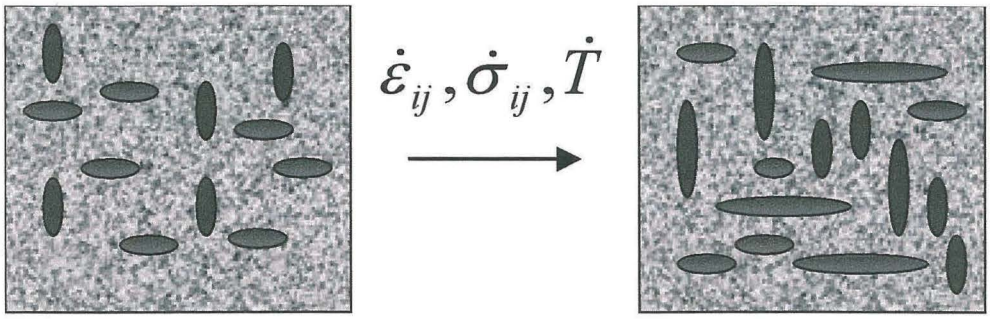

Figure 3.0 Schematic representation of the growth of flaws or cracks in a material subjected to arbitrary mechanical or thermal loading.

Let $\dot{\sigma}_{ij}$ be the Cauchy stress rate tensor and let $\dot{\varepsilon}_{ij}$ be the small strain rate tensor. Assuming isotropic behavior, we may separate the Cauchy stress rate and small strain rate into the deviatoric and dilatational tensor quantities. It should be noted that this separation only applies to the isotropic case and will not be valid when an anisotropic model is later developed. Let $\dot{s}_{ij}$ and $\dot{e}_{ij}$ be the deviatoric Cauchy stress rate tensor and the deviatoric rate of deformation, or *"small strain rate"* tensor, respectively, where

$$\dot{e}_{ij} = \dot{\varepsilon}_{ij} - \frac{1}{3}\dot{\varepsilon}_{kk}\delta_{ij} \tag{3.1}$$

$$\dot{s}_{ij} = \dot{\sigma}_{ij} - \frac{1}{3}\dot{\sigma}_{kk}\delta_{ij} \tag{3.2}$$

Using the principal of superposition of strains, it is assumed that the total deviatoric strain is the sum of the elastic deviatoric strain e^e_{ij} and a strain e^c_{ij} that is defined as the cracking strain:

$$e_{ij} = e^e_{ij} + e^c_{ij} \tag{3.3}$$

Equation 3.3 may also be expressed in rate form as

$$\dot{e}_{ij} = \dot{e}^e_{ij} + \dot{e}^c_{ij} \tag{3.4}$$

In an effort to define the cracking strain rate simply but robustly, a few relationships from statistical crack mechanics are employed. The fundamental cracking relationship relates the crack strain to the average crack radius, a (i.e. crack size):

$$e_{ij}^{c} = \beta^{e} a^{3} s_{ij} \tag{3.5}$$

where the constant β^{e}, for compressive loading, is defined by the relation:

$$2G\beta^{e} = \frac{256\pi}{15}\frac{(5-\nu)(1-\nu)}{(2-\nu)}N_{o} \tag{3.6}$$

where G is the shear modulus, and N_o is the number of cracks per unit volume. The quantities in 3.14 can be used to define a length scale parameter, C, related to the crack spacing:

$$2G\beta^{e} = \frac{256\pi}{15}\frac{(5-\nu)(1-\nu)}{(2-\nu)}N_{o} = \left(\frac{1}{C}\right)^{3} \tag{3.7}$$

Combining equations 3.3 - 3.7 results in the simplified form

$$2Ge_{ij}^{c} = \left(\frac{a}{C}\right)^{3} s_{ij} \tag{3.8}$$

The term (a/C) represents volumetric damage due to a distribution of cracks with an average size a. Rearrangement of equation 3.16 and differentiation with respect to time leads to the relation

$$\dot{e}_{ij}^{c} = \frac{1}{2G}\left[3\left(\frac{a}{C}\right)^{2}\left(\frac{\dot{a}}{C}\right)s_{ij} + \left(\frac{a}{C}\right)^{3}\dot{s}_{ij}\right] \tag{3.9}$$

Equation 3.9 states that the cracking strain rate is a function of the crack size, a, the crack speed, $\dot{a}$, the deviatoric stress rate, $\dot{s}_{ij}$ and the deviatoric state of stress s_{ij}. This gives the model the capability to predict rate sensitive damage. The deviatoric response now becomes

$$\dot{s}_{ij} = 2G\dot{e}_{ij} - \left[3\left(\frac{a}{C}\right)^{2}\left(\frac{\dot{a}}{C}\right)s_{ij} + \left(\frac{a}{C}\right)^{3}\dot{s}_{ij}\right] \tag{3.10}$$

The above equations provide the general framework for the model. In order to determine the evolution of the microcrack length, a, with time, appropriate fracture criteria for crack initiation and growth must be incorporated. The applied stress intensity factor is related to the effective stress, σ, and crack length by:

$$K_{I}^{d}(t) = \sigma(t)\sqrt{\pi a(t)} \tag{3.11}$$

Using equation 3.11 for a given configuration, the instantaneous values of K_I^d and $\dot{K}_I^d$ can be computed. The incorporation of fracture criteria for initiation and growth for a given material will yield predictions of the extent of damage sustained under a given loading history.

An evolution equation for the crack growth rate $\dot{a}$ is required to complete this part of the model. We assume the crack growth rate depends on the dynamic stress intensity as shown in schematically in Figure 3.1. Figure 3.1 is only a general statement, and does not define the crack speed vs. dynamic stress intensity factor for all brittle materials.

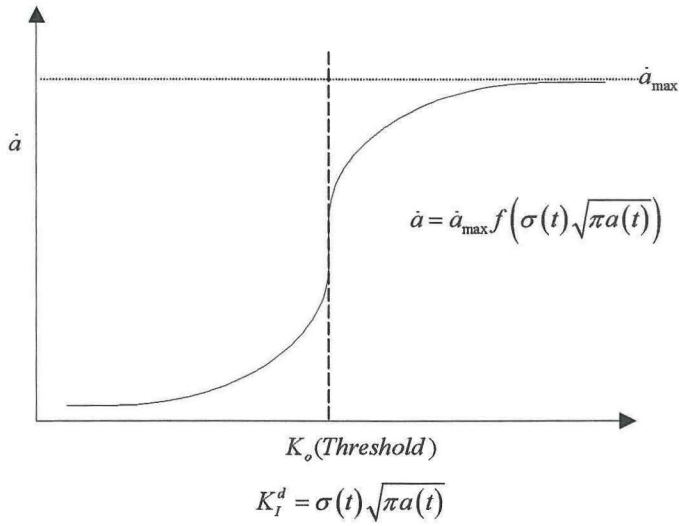

Figure 3.1 The crack growth rate relationship shown schematically.

Having developed the deviatoric response incorporating the dynamic fracture criteria for initiation and growth, a simplified dilatational response was assumed. This dilatational response was assumed to be purely elastic and was given simply by

$$\sigma_m = \kappa \varepsilon_{ii} \tag{3.12}$$

where κ is the bulk modulus. The total stress rate is the sum of the deviatoric and dilatational stress rates, equations 3.10 and 3.12, respectively, or

$$\dot{\sigma}_{ij} = \dot{s}_{ij} + \dot{\sigma}_m \delta_{ij} \tag{3.13}$$

where δ_{ij} is the Kronecker delta. It should be noted that the above simple model is strictly accurate for compression. For tension and multiaxial stress states it can be generalized as described in Bennett *et al.* (1998).

The micormechanical constitutive model was applied to the Dionysus-Pentelicon marble using the appropriate material properties from Table 2.0. In addition, approximate crack initiation and growth criteria were estimated as described in the previous section.

Table 3.0 Parameters used in the micromechanical constitutive model.

Parameters used in the model.

Initial Crack Size *ai*= 20 microns
Elastic Modulus *E*= 70 MPa
Normalization Parameter, *C*=(1.1e4)ai
Poissons Ratio $v = 0.33$
Shear Wave Speed, $Cs = 3200$ m/s
Longitudinal Wave Speed, $Cl = 6100$ m/s
Raleigh Wave Speed, $Cr = Cs*(0.862+1.14*v)/(1+v) = 2980$ m/s

Dynamic Stress Intensity, K_I^d	Crack Growth Rate, $\dot{a}$
0	0
0.98Ko	1e-3
1.02*Ko*	0.39*amax*
1.5*Ko*	0.43*amax*
2.0*Ko*	0.43*amax*
1000*Ko*	

It should be recognized, however, that these initial simulations are only intended to provide a means to assess whether or not the model can be used to capture the qualitative features of the dynamic constitutive behavior reported in Section 2.0. More detailed simulations incorporating the measured fracture criteria will be performed after these data have been obtained as part of the extended experimental program.

The stress – strain response was investigated by prescribing the strain rate and performing an Euler integration of Equation 3.13. Figure 3.2 shows a summary of these simulations, plotting the peak stress as a function of strain rate.

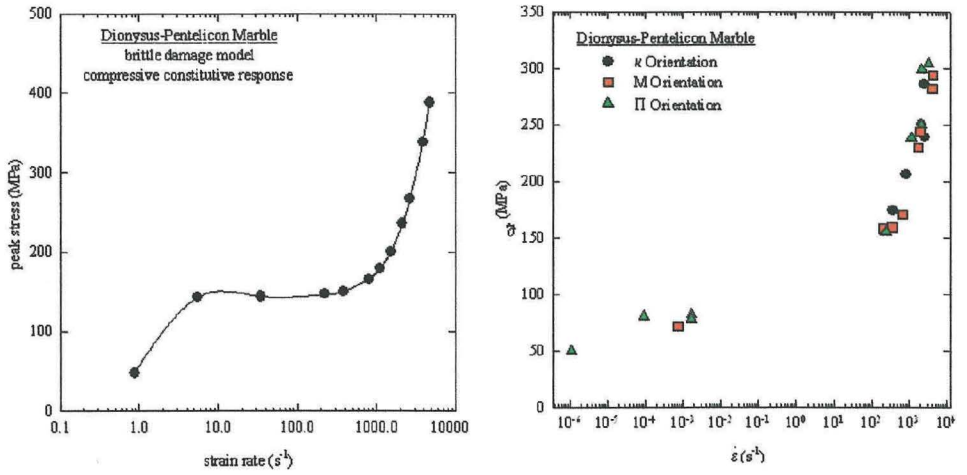

Figure 3.2 A plot of the predicted and experimental values of peak or failure stress with strain rate.

Comparing the simulation results in Figure 3.2 to the experimental results in Figure 2.5 reveals many very similar features. First, the order of magnitude of the peak stress is similar, ranging from ~50 to 350 MPa over the same range of strain rate. Second, the shapes of the curves are similar. At the lowest strain rates, there is an initial increase in the failure stress, whereas at intermediate strain rates the failure stress is approximately constant. Under dynamic loading, there is a dramatic increase in the failure stress such that at the highest strain rates the peak stress has increased by a factor of 7 in comparison to the static strength. It is clear from the results presented in Figure 3.2 that the model can adequately capture the general features of the experimentally determined constitutive response.

Future work in this area will utilize the accurate dynamic fracture toughness measurements on marble and more elaborate crack growth criteria to "calibrate" the model rigorously and to capture the many salient features of the constitutive / damage behavior of marble.

4.0 Preliminary Finite Element Simulations

The constitutive model presented in Section 3.0 was implemented into the nonlinear lagrangian finite element code DYNA3D (1989) and exercised on several dynamic impact experiments. Several of these experiments were also performed in the laboratory during the initial investigation of the dynamic response of the marble. The preliminary finite element simulations are intended to be used for more qualitative comparison rather than quantitative. The goal of these preliminary simulations is to exercise the constitutive model in 3D and to identify deficiencies or modifications that must be included in order for the model to adequately represent the complete behavior of the marble.

DYNA3D(1998) is a three dimensional nonlinear lagranagian explicit finite element code. It is mainly used to simulate the nonlinear dynamic response of solids and structures. DYNA3D is also a legacy code, meaning that it has been in use for the past 20 years and may be obtained free of charge from Lawerence Livermore National Laboratory. This code is used throughout industry. It is recommended that anyone interested in the details of implementing a material or constitutive model into this particular code should review the users manual.

4.1 Plate Impact Simulations

The first impact simulation involves an impact on the front of side of a 3x3x1/2 inch marble plate by a 1 inch diameter steel ball with an impact velocity of 40 m/s. . The steel ball was modeled as a linear elastic material and contains about 10,000 elements. The plate was modeled using the constitutive model presented in Section 3.0. Both object were discretized using 8 node hex elements as shown in Figure 4.10 The finite element model of the plate contains roughly 50,000 elements. Several view of the finite element model is shown in Figure 4.0.

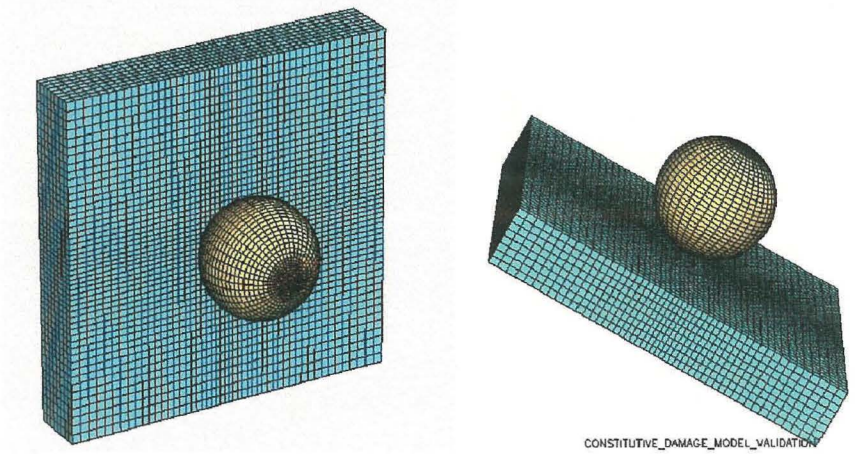

Figure 4.10 Isometric and side view of the plate impact mesh.

Figures 4.11 – 4.13 show the relative cracking damage *(a/C)* at three different times during the simulation.

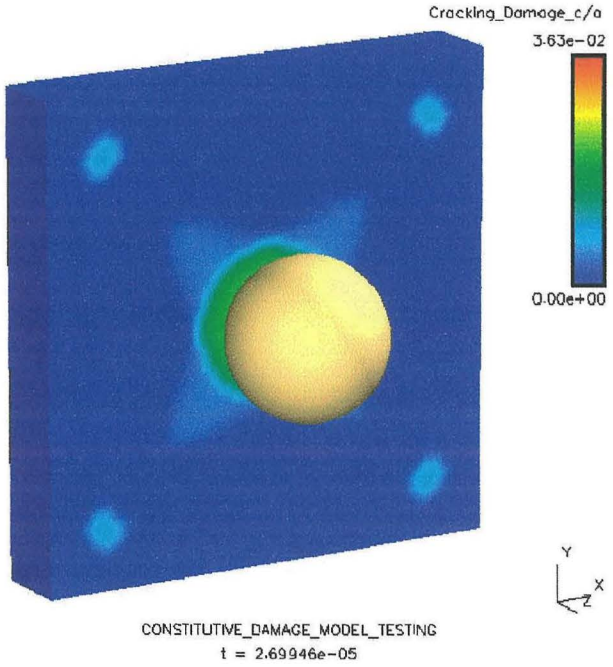

Figure 4.11a Front view, relative cracking damage, 26.9 microseconds after impact.

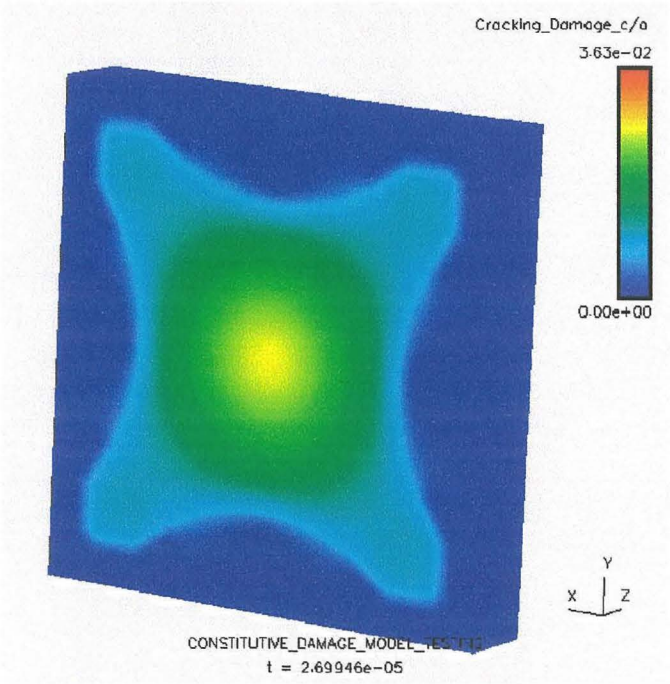

Figure 4.11b Back view, relative cracking damage, 26.0 microseconds after impact.

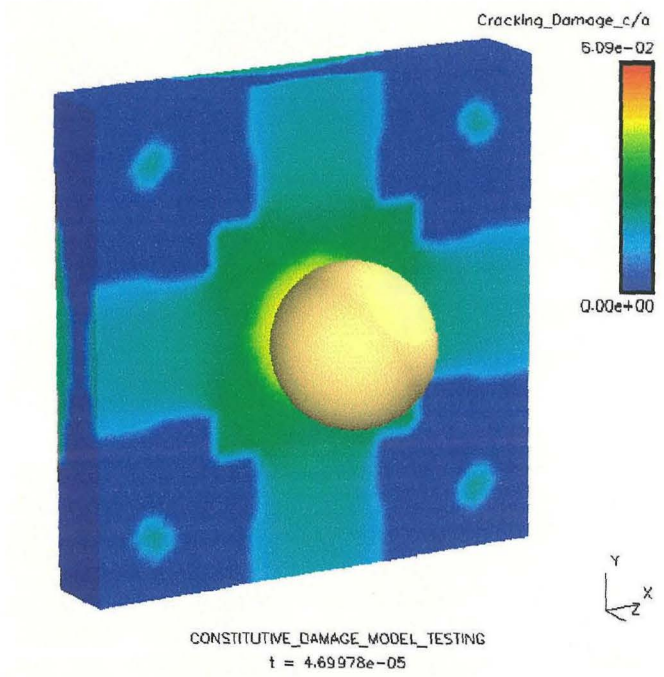

Figure 4.12a Front view, relative cracking damage, 46.9 microseconds after impact.

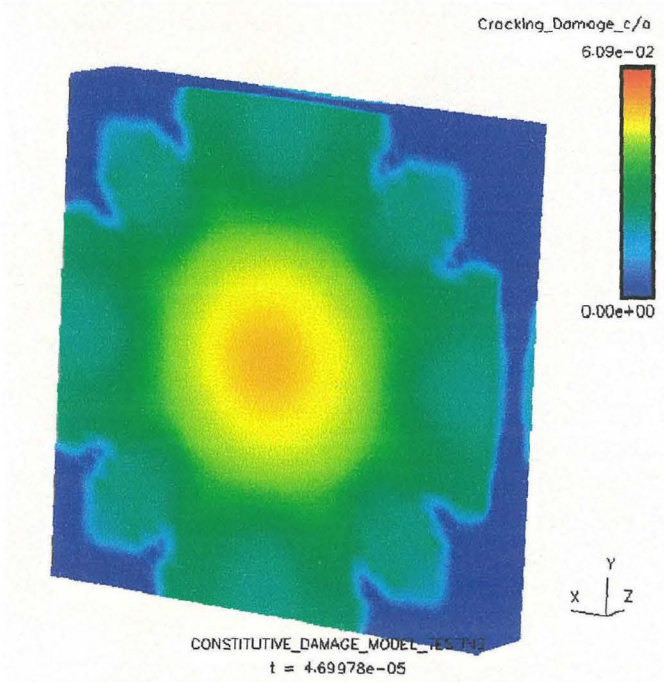

Figure 4.12b Back view, relative cracking damage, 46.9 microseconds after impact.

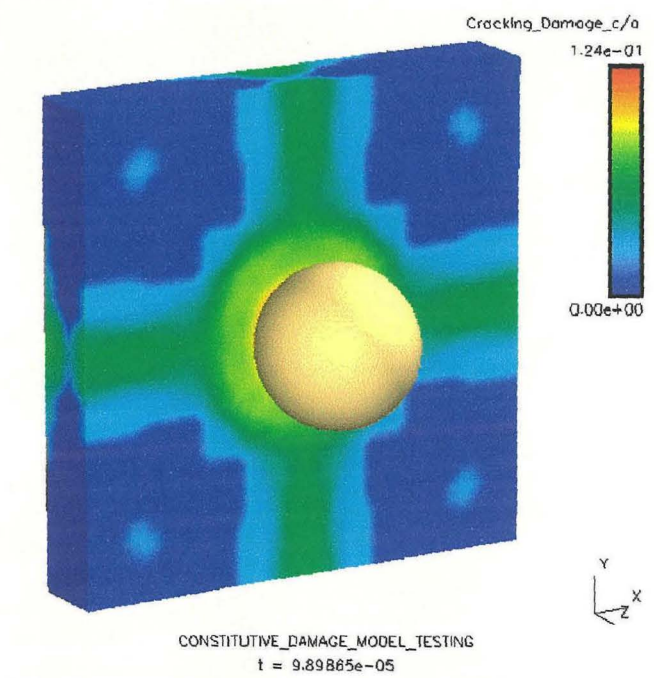

Figure 4.13a Front view, relative cracking damage, 98.9 microseconds after impact.

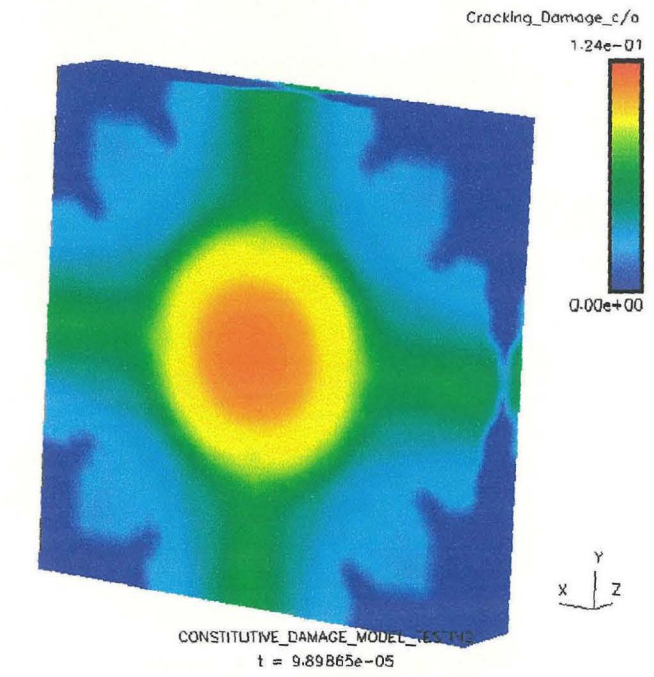

Figure 4.13b Back view, relative cracking damage, 98.9 microseconds after impact

Figure 4.14 is a photograph of the fragmented tile looking at the imaged surface, or the surface opposite the impact. The central damaged region is conical: all the material initially within the cone was pulverized completely as a result of impact. The pieces that remained intact were split by cracks running radially from the center of the specimen. These cracks occurred at roughly equivalent angular intervals of 33° around the middle of the tile.

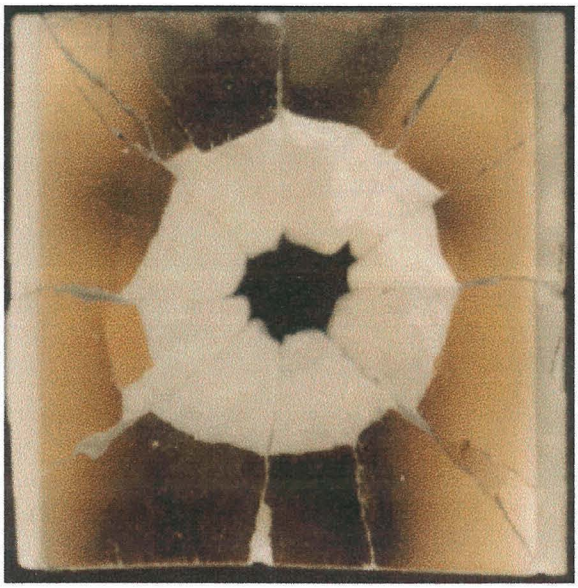

Figure 4.4, A photograph of the fragmented marble tile impacted at 40 m s^{-1}, from Rosakis (1999)

We can see that the simulation was reasonably able to represent the experimentally observed damage. The observation of wide-spread damage justifies the application of continuum damage models (based on microcracking) of the type discussed in Section 3.0.

4.2 Column Impact Simulation

The second impact simulation involves an impact of a cannon ball on the front of side of a section of a marble column shown in Figure 4.2. This experiment has not been performed in the laboratory to date, however, during the siege in 1687 numerous columns of the Parthenon were impacted by cannon balls. This simulation is being performed mainly for its relevance to the final goal of the project, which is to simulate the actual damage present in the structure after the cannon ball assault and resulting explosion. The projectile was modeled as linear elastic isotropic material and the marble column was modeled using the material model presented in Section 3.0. The projectile is 4 in. in diameter and the marble section is 4.5 ft. in diameter. The projectile velocity for the normal and oblique impact cases is 175 m/s.

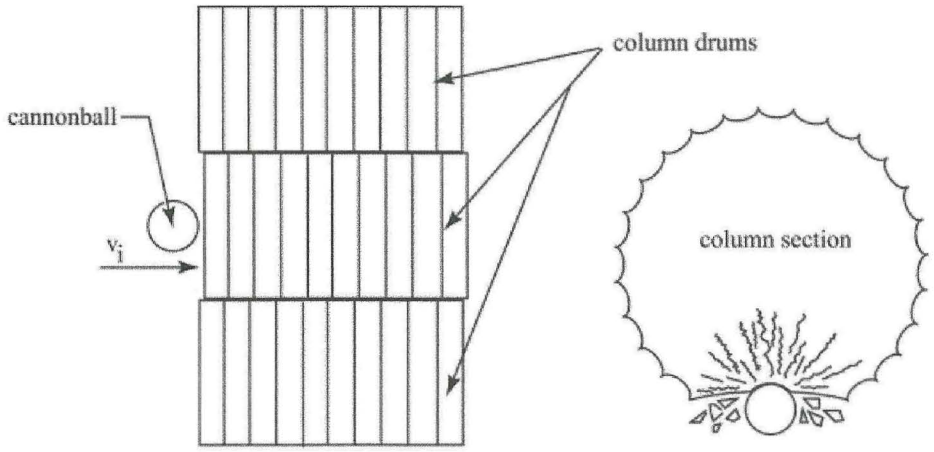

Figure 4.20 Cannon ball impact on marble columns of the Parthenon, from Rosakis (1999)

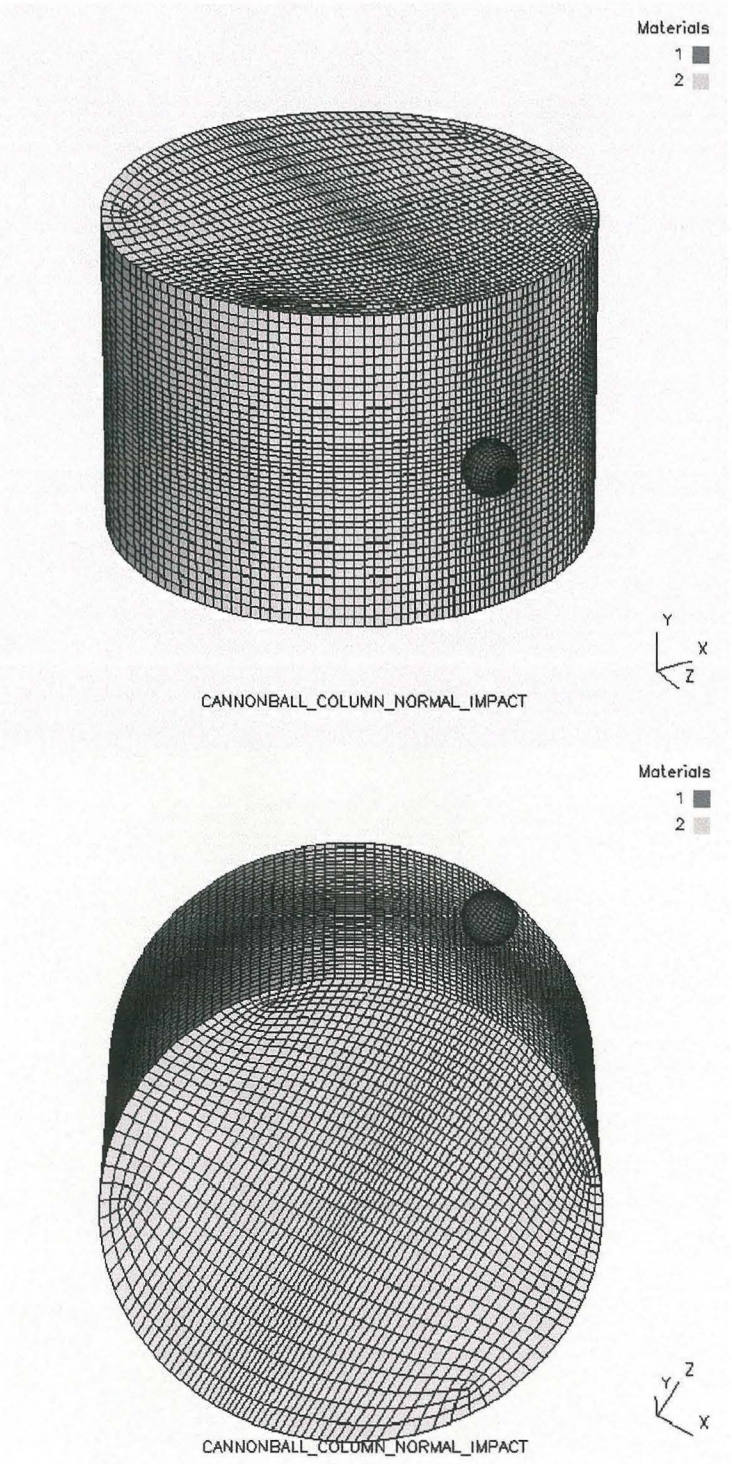

Figure 4.21 Isometric and side view of the finite element model.

Figures 4.22 – 4.24 show the relative cracking damage *(a/C)* at three different times during the simulation for normal and oblique projectile impacts.

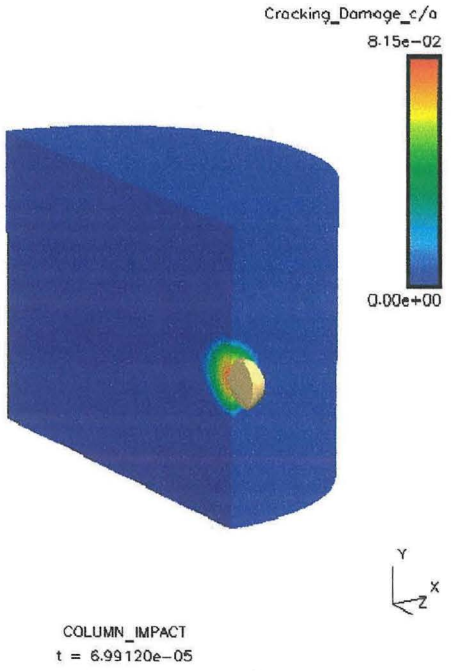

Figure 4.22a Cutaway view for a normal impact showing relative cracking damage at 69.9 microseconds after impact.

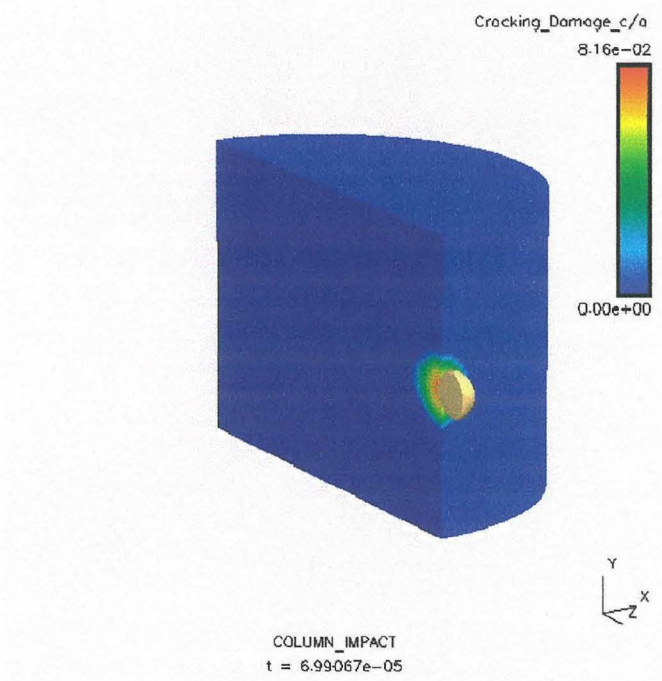

Figure 4.22b Cutaway view for a 45° oblique impact showing relative cracking damage at 69.9 microseconds after impact.

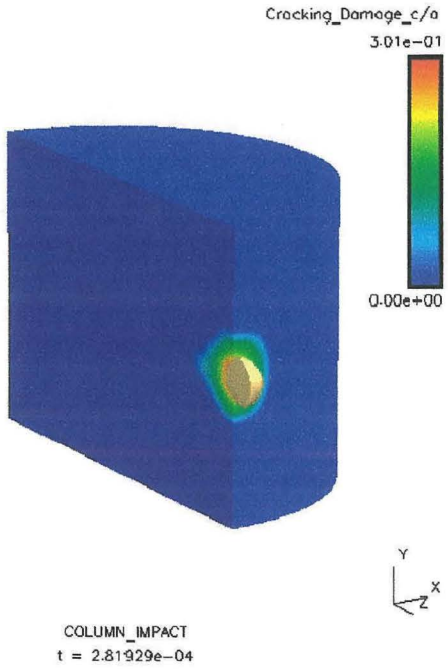

Figure 4.23a Cutaway view for a normal impact showing relative cracking damage at 281.9 microseconds after impact.

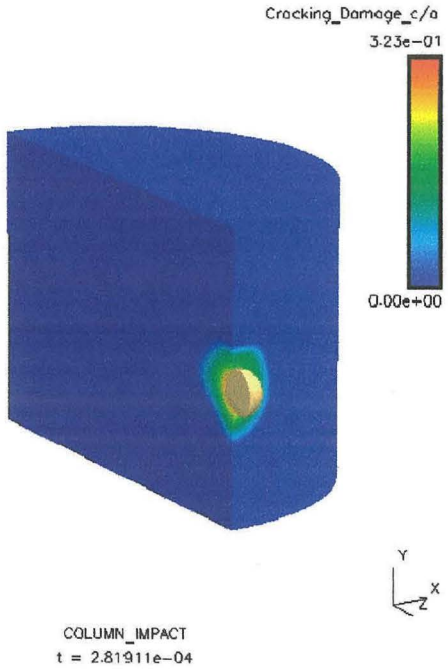

Figure 4.23b Cutaway view for a 45° oblique impact showing relative cracking damage at 281.9 microseconds after impact.

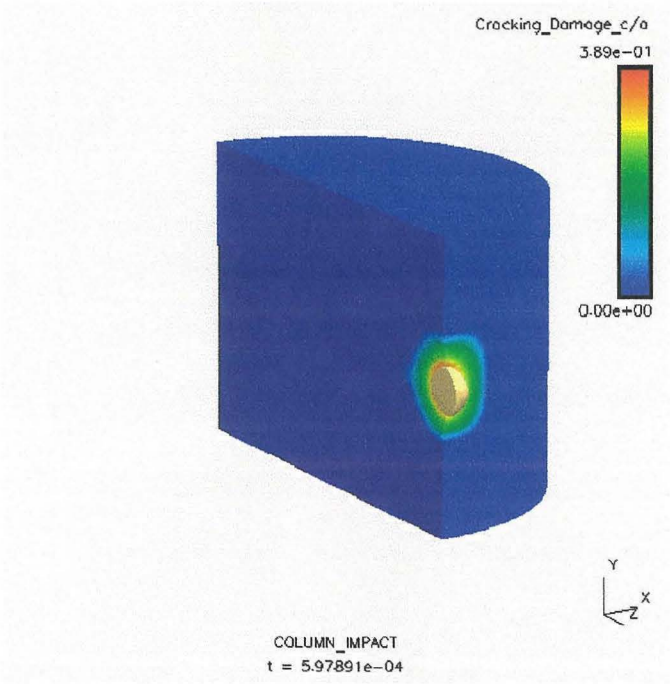

Figure 4.24a Cutaway view for a normal impact showing relative cracking damage at 597.87 microseconds after impact.

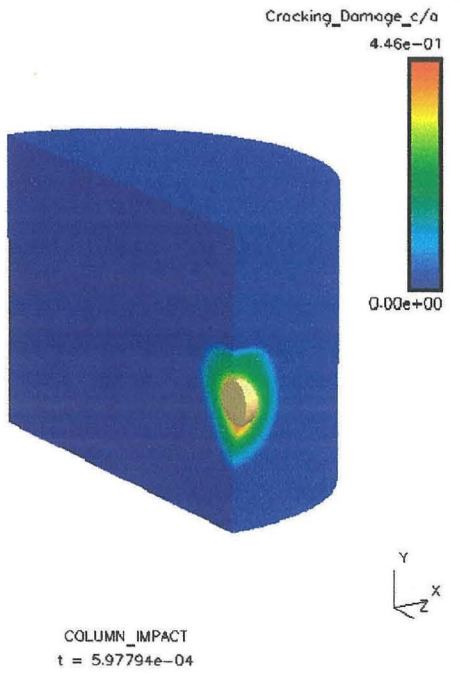

Figure 4.24b Cutaway view for a 45° oblique impact showing relative cracking damage at 597.8 microseconds after impact.

Due to the fact that this experiment has not been performed since 1678 experimental evidence is limited to photographs of the impact craters on the columns of the Parthenon shown in Figure 4.25 and Figure 4.26.

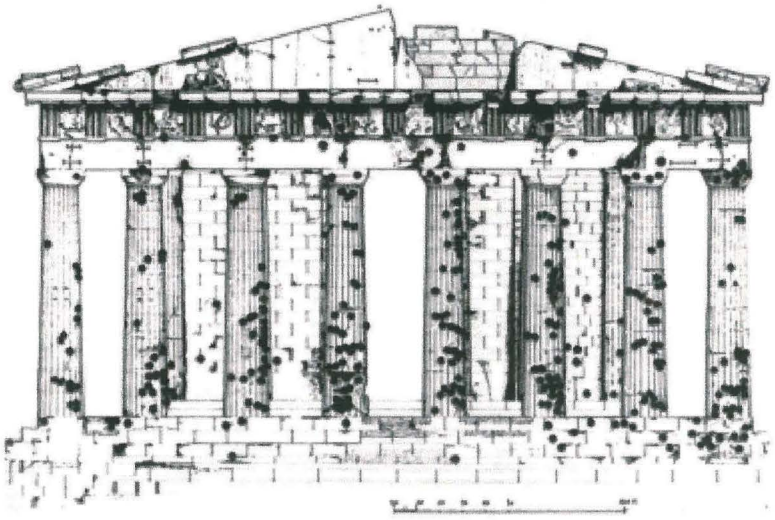

Figure 4.25 Cannonball damage to the Parthenon (a) schematic drawing of the extent and location of cannonball damage on the western side indicated by the black circles, from Economakis

Figure 4.26 Photograph of an indentation and cracks caused by the impact of a cannonball on one of the marble columns and a photograph of one of Morosini's cannon balls, from Economakis

4.3 Chevron Notch Plate Impact Simulations

This experiment was originally used to initiate a normal mode failure in fiber reinforced composite. Because of its popularity, it has been used to investigate dynamic failure of other materials, such as marble. The experiment consists of a marble specimen attached to a steel metal strip, which is impacted with a steel projectile at 20 m/s. The specimen was approximately 88 mm wide and 150 mm long. The marble specimen was modeled using the constitutive model presented in Section 3.0. The steel metal strip and the steel projectile were modeled using a linear elastic isotropic model.

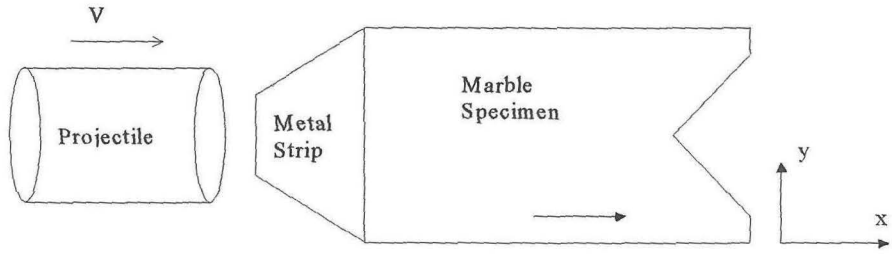

Figure 4.30 Modified plate impact geometry.

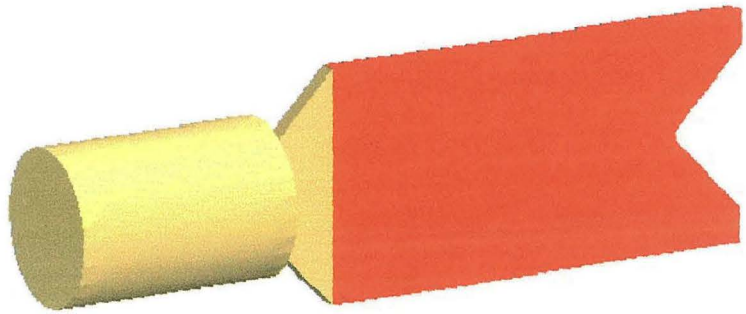

Figure 4.31 Chevron notch impact, actual finite element model, 70,000 elements in the marble specimen.

Figures 4.32 – 4.34 show the relative cracking damage *(a/C)* at three different times during the simulation.

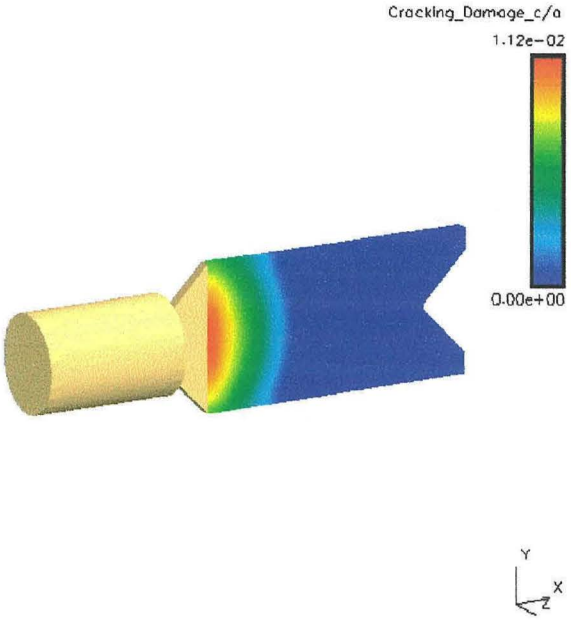

Figure 4.32 Chevron notch impact simulation showing relative cracking damage at 20.4 microseconds after projectile impact.

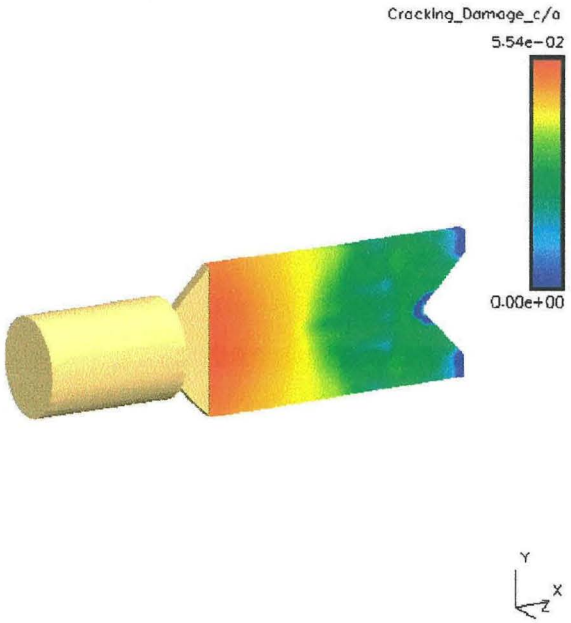

Figure 4.33 Chevron notch impact simulation showing relative cracking damage at 56.9 microseconds after projectile impact.

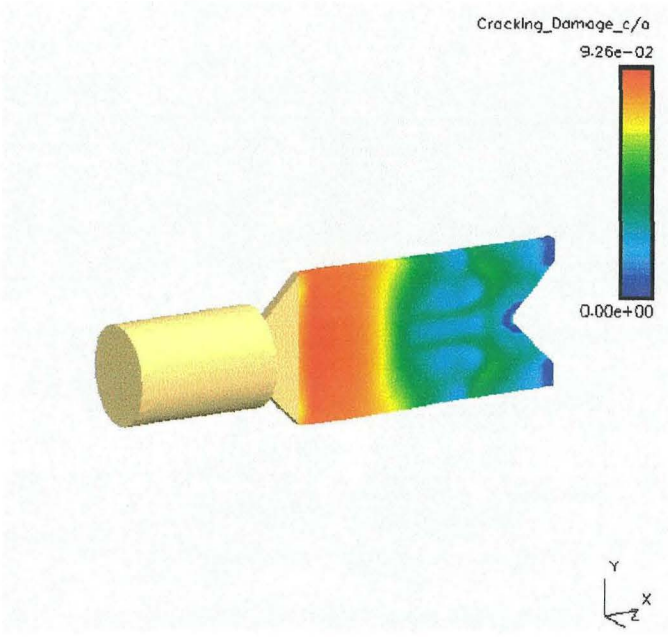

Figure 4.34 Chevron notch impact simulation showing relative cracking damage at 89.9 microseconds after projectile impact.

Figure 4.35 is a photograph of the untested specimen and also of the post-mortem state. In the fractured specimen, the extensive damage near the notch tip is apparent with much of the material directly ahead of and below the notch having been completely pulverized. There was also extensive damage near the impacted edge of the specimen, to the right. Perhaps the most interesting feature of the fractured specimen is that the cracks just above and below the main crack, as observed in the high-speed images in Figure 4.36, did not lead to the formation of specimen fragments. In other words, these branched cracks were not sufficiently deep or long to separate the material through the thickness. This indicates that in many cases microcracking and damage may be highly localized, thereby not leading to gross failure. Nevertheless, the structural integrity of the remaining marble pieces is undoubtedly considerably less than the original specimen. The observation of wide-spread damage justifies the application of continuum damage models (based on microcracking) of the type discussed in the following section.

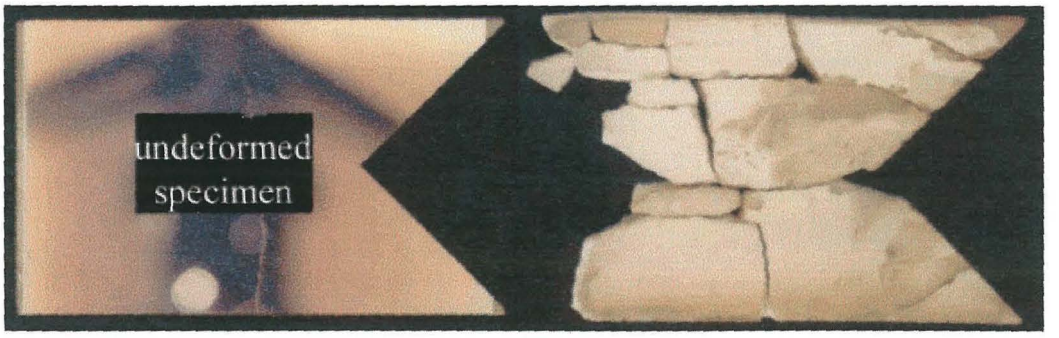

Figure 4.35 Undeformed Chevron notch specimen and fractured specimen impacted at a speed of 20 m/s, from Rosakis (1999)

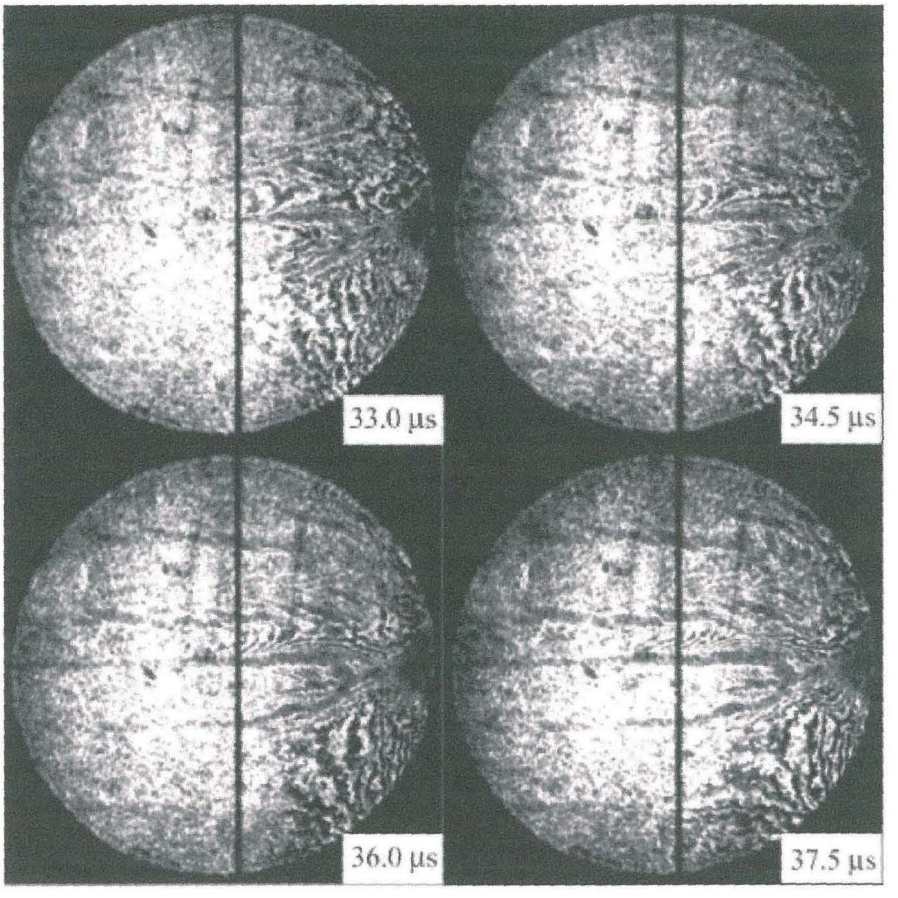

Figure 4.36 Selected sequence of four consecutive Twyman-Green interferograms recorded after the initiation of crack growth. The specimen was impacted at a speed of 17 m/s, from Rosakis (1999)

We can see that the simulation is reasonably able to represent the experimentally observed damage. It should be once noted that this experiment involved discrete fracture of the specimen and the constitutive model approach is unable to predict this event.

5.0 Conclusions

The constitutive model described here relates deformation and failure processes on the macroscopic and mesoscopic scales. The approach described in formulating the model provides a way to account for microstructure and phenomena that are not accessible to macroscopic calculations. The model was formulated with the intent to implement it into a three dimensional nonlinear lagrangian finite element code. This capability once completely validated would be used to simulate the response of large structures composed of Dionysus-Pentelicon marble undergoing impact and blast loading. The resulting damage predictions would be used to assess the overall damage inflicted on the structure and to use this knowledge for restoration efforts. The observation of wide-spread damage occurring in the experiments presented in Section 4.0 justifies the application of continuum damage models (based on microcracking) of the type discussed in Section 3.0. Based on the results of Section 4.0 we can see that the constitutive model is reasonably able to represent the experimentally observed damage.

6.0 References

Addessio, F.L. and J.N. Johnson (1990) A constitutive model for the dynamic response of brittle materials. *J. Appl. Phys.*, **67**, 3275.

Barrenblatt, G. I. (1962) The mathematical theory of equilibrium cracks in brittle fracture. *Adv. Appl. Mech.* 7, 55.

Bennett, J.G., K.S. Haberman, J.N. Johnson, B.W. Asay and B.F. Henson (1998) A constitutive model for the non-shock ignition and mechanical response of high explosives. *J. Mech. Phys. Solids*, **46**, 2303.

Camacho, G. T. and M. Ortiz (1996) Computational modeling of impact damage in brittle materials. *Int. J. Solids Struct.* **33**, 2899.

Chen W.-N. and G. Ravichandran (1997) Dynamic compressive failure of a glass ceramic under lateral confinement. *J. Mech. Phys. Solids*, **45**, 1303.

Coker, D. and A.J. Rosakis (1998a) Dynamic crack initiation in unidirectional graphite-epoxy composite materials. Presented at *U.S. National Congress of Applied Mechanics*, Gainsville, Florida.

Coker, D. and A.J. Rosakis (1998b) Experimental observations of intersonic crack growth in asymmetrically loaded, unidirectional composite plates, GALCIT-SM Report 98-16.

Dienes, J.K. (1984) Frictional hot spots and propellant sensitivity. *Proc. Mater. Res. Soc.*, **24**, 125.

Dugdale, D. S. (1960) Yielding of steel sheets containing slits. *J. Mech. Phys. Solids* **8**, 100.

Economakis, R. (1994) *Acropolis Restoration: The CCAM Interventions*, Academy Editions, London.

Haberman, K.S., B.W. Asay, B.F. Henson and D.J. Funk (1997) Modeling, simulation and experimental verification of constitutive models for energetic materials. Presented at *APS Topical Conference on Shock Compression of Condensed Matter*, Amherst, Massachusetts.

Heinrich, H. (1990) *Die Explosion des Parthenon*, Schoenwald Druck, Berlin.

Huang, Y., W. Wang, C. Liu and A.J. Rosakis (1999) Analysis of intersonic crack growth in unidirectional fiber-reinforced composites. *J. Mech. Phys. Solids*, accepted for publication.

Liu, C., W.G. Knauss, and A.J. Rosakis (1998) Loading rates and the dynamic initiation toughness in brittle solids. *Inter. J. Fracture*, **90**, 103.

Meyers, M. A. (1994) *Dynamic Behavior of Materials*, Wiley & Sons, New York.

Oguni, K. and G. Ravichandran (1998) Dynamic behavior of fiber reinforced composites under multiaxial compression. *Experimental Mechanics Advances in Design, Testing & Analysis, Proceedings of the 11th International Conference, Oxford, 24-28 August, 1998*, (I.M. Allison, editor) Ashgate, Brookfield, Vermont, p. 211.

Owen, D.M., S.-M. Zuang, A.J. Rosakis and G. Ravichandran (1999) Experimental determination of dynamic crack initiation and propagation fracture toughness in thin aluminum sheets. *Inter. J. Fracture*, **90**, 153.

Ravi-Chandar, K. and W.G. Knauss (1984) An experimental investigation into dynamic fracture: I. Crack initiation and arrest. *Inter. J. Fracture,* **25**, 247.

Rice, J. R. (1968) Mathematical analysis in the mechanics of fracture. *Fracture* (H. Leibowitz, editor) Academic Press, p. 191.

Rosakis, A.J. (1993) Two optical techniques sensitive to gradients of optical path difference: The method of caustics and the coherent gradient sensor (CGS), in *Experimental Techniques in Fracture*, (J.S. Epstein, editor), Wiley & Sons, New York, p. 327.

Rosakis, A.J., O. Samudrala and D. Coker (1999) Cracks faster than the shear wave speed. *Science*, **284**, 1337.

Rosakis, A.J., C. Liu, M.G. Stout and R.W. Ellis (1999) Observations of transonic shear and opening cracks in unidirectional composites containing cutouts and holes. In preparation

Walter, M.E., D.M. Owen, and G. Ravichandran (1994) Static and dynamic tension testing of ceramics and ceramic composites. *Mechanical Testing of Ceramics and Ceramic Composites; Proceedings of the International Mechanical Engineering Congress and Exhibition, Volume 197* (A. Gilat, editor) American Society of Mechanical Engineering, New York, N.Y., p. 13.

Zehnder, A.T. and A.J. Rosakis (1990) Dynamic fracture initiation and propagation in 4340 steel under impact loading. *Inter. J. Fracture,* **43**, 271.